CURRENT STAR FORMATION IN THE PERSEUS MOLECULAR CLOUD: CONSTRAINTS FROM UNBIASED SUBMILLIMETER AND MID-INFRARED SURVEYS

Jes K. Jørgensen,[1] Doug Johnstone,[2,3] Helen Kirk,[3,2] and Philip C. Myers[1]

ABSTRACT

We present a census of the population of deeply embedded young stellar objects (YSOs) in the Perseus molecular cloud complex based on a combination of *Spitzer Space Telescope* mid-infrared data from the Cores to Disks (c2d) legacy team and JCMT SCUBA submillimeter maps from the COMPLETE team. The mid-infrared sources detected at 24 μm and having $[3.6] - [4.5] > 1$ are located close to the center of the SCUBA cores, typically within $15''$ of their peaks. The narrowness of the spatial distribution of mid-infrared sources around the peaks of the SCUBA cores suggests that no significant dispersal of the newly formed YSOs has occurred. This argues against the suggestion that motions of protostars regulate the timescales over which significant (Bondi-Hoyle) accretion can occur. The YSOs are found to have red $[3.6] - [4.5]$ and $[8.0] - [24]$ colors, but not comparable red $[5.8] - [8.0]$ colors. The most deeply embedded YSOs are found in regions with high extinction, $A_V \geq 5$, similar to the extinction threshold observed for the SCUBA cores. All the SCUBA cores with high concentrations have embedded YSOs, but not all cores with low concentrations are starless. From the above considerations, a relatively unbiased sample of 49 deeply embedded YSOs is constructed. Embedded YSOs are found in 40 of the 72 SCUBA cores, with only three cores harboring multiple embedded YSOs within $15''$. The equal number of SCUBA cores with and without embedded YSOs suggests that the timescale for the evolution through the dense prestellar stages, where the cores are recognized in the submillimeter maps and have central densities of $5 \times 10^4 - 1 \times 10^5$ cm^{-3}, is similar to the timescale for the embedded protostellar stages. The current star formation efficiency of cores is estimated to be approximately 10%–15%. In contrast, the star formation efficiency averaged over the cloud lifetime and compared to the total cloud mass is only a few percent, reflecting also the efficiency in assembling cloud material into the dense cores actually forming stars.

Subject headings: ISM: clouds — ISM: evolution — stars: formation — stars: pre–main-sequence

1. INTRODUCTION

Any theory of low-mass star formation should not only be able to make predictions for one characteristic stage, such as the core mass spectrum in molecular clouds or the initial mass function of emerging stars, but also relate those through both pre- and protostellar stages. A number of very basic questions of star formation still remain unanswered and debated (see, e.g., Di Francesco et al. [2007], Ward-Thompson et al. [2007], and Ballesteros-Paredes et al. [2007] for recent reviews and discussions of both observational and theoretical studies), which can be addressed with large homogeneous surveys from mid-infrared through (sub)millimeter wavelengths and well-defined lists of sources such as those presented in this paper. For example, is the star formation process highly dynamical, with cores being transient phenomena in a turbulent medium, and are protostars only accreting in short periods of time when "passing by" these dense environments (i.e., Bondi-Hoyle accretion)? Or is low-mass star formation a more slowly evolving process, as preferred in traditional ambipolar diffusion scenarios, and in that case, how important are other effects, such as turbulence, in regulating the speed at which the process occurs? How efficient is the star formation process in turning prestellar dust and gas into young stars? Are there specific relationships between the natal prestellar cores and the emerging protostars; for example, do the properties of prestellar cores reflect in whether a given core actually forms a star and perhaps whether it forms a single or multiple system? Many of these discussions hinge on

statistical arguments, for example, estimates of the evolutionary rate of protostars through counts of the number of YSOs in different stages. Previous studies of the deeply embedded stages were hampered by low-sensitivity single-element (sub)millimeter receivers and confusion in low-resolution, low-sensitivity infrared observations, such as those from the *Infrared Astronomical Satellite* (*IRAS*) and *Infrared Space Observatory* (*ISO*). In the last few years systematic, detailed surveys of larger regions have been made possible using wide-area imaging at high resolution and sensitivity using submillimeter telescopes, such as the James Clerk Maxwell Telescope (JCMT) with the Submillimeter Common User Bolometer Array (SCUBA), and mid-infrared telescopes, including the *Spitzer Space Telescope* and its Infrared Array Camera (IRAC) and Multiband Imaging Photometer (MIPS). In this paper we present a census of the deeply embedded low-mass protostars in the Perseus molecular cloud utilizing recently obtained large-scale *Spitzer* c2d (Jørgensen et al. 2006; Rebull et al. 2006) and JCMT SCUBA maps (Kirk et al. 2006) and discuss some of the strong constraints for theories of low-mass star formation emerging from these homogeneous data sets.

The earliest, most deeply embedded stages of low-mass protostars or the latest stages of prestellar cores close to the onset of collapse are important for insight into the physical conditions regulating low-mass star formation. Approaching the problem from the prestellar stages, continuum observations provide strong constraints on the distribution of dust and, by inference, the gas, in star-forming regions. In particular, large-scale mapping with submillimeter and millimeter wavelength continuum bolometers (e.g., Motte et al. 1998; Johnstone et al. 2000, 2004; Hatchell et al. 2005; Enoch et al. 2006; Kirk et al. 2006; Young et al. 2006) has enabled relatively unbiased tabulations of dust condensations that either just have formed or are likely to form protostars. The

[1] Harvard-Smithsonian Center for Astrophysics, Cambridge, MA; jjorgensen@cfa.harvard.edu.
[2] Herzberg Institute of Astrophysics, National Research Council of Canada, Victoria, BC, Canada.
[3] Department of Physics and Astronomy, University of Victoria, BC, Canada.

distribution of dust emission can also be used to infer the column density distribution of the dust in both pre- and protostellar cores and from there potentially derive self-consistent density and temperature distributions through detailed radiative transfer modeling (e.g., Hogerheijde & Sandell 2000; Evans et al. 2001; Jørgensen et al. 2002; Shirley et al. 2002). Alternatively, observed parameters, such as peak flux or size, can be used as empirical diagnostics to estimate which cores will undergo collapse (e.g., Johnstone et al. 2000; Kirk et al. 2006).

The dust continuum maps themselves do not answer the question whether a given core already has formed a central protostar; for that, deep mid-infrared observations are needed. Furthermore, mid-infrared observations are important as an evolutionary indicator once the protostar itself has formed; its infrared excess, spectral slope in the mid-infrared range, or combination of colors are typically used to distinguish between objects in different stages (e.g., Lada 1987; Greene et al. 1994; Allen et al. 2004). Still, the infrared colors themselves do not provide an unambiguous mapping to object type and/or evolutionary status. Deeply embedded YSOs, for example, share many of the same spectral energy distribution (SED) characteristics as more evolved edge-on disk systems. Also, since the most deeply embedded YSOs emit a significant fraction of their luminosity at far-infrared and submillimeter wavelengths (Class 0 objects are, for example, observationally defined as objects emitting more than 0.5% of their total luminosity at wavelengths longer than 350 μm; e.g., André et al. 1993, 2000), establishing their full SEDs through these wavelengths is important. All of these issues illustrate the importance of combining submillimeter and mid-infrared observations as is done in this paper.

The *Spitzer Space Telescope* From Molecular Cores to Planet Forming Disks (c2d; Cores to Disks) legacy team (Evans et al. 2003) has surveyed five of the nearby star-forming clouds using the mid-infrared cameras, IRAC and MIPS, with the aim of characterizing the ongoing star formation in each. The Coordinated Molecular Probe Line Extinction Thermal Emission (COMPLETE) survey of star-forming regions (Goodman et al. 2004; Ridge et al. 2006) collects data for the three northern of these regions over a range of molecular lines, extinction, and dust continuum. In this paper we combine the information from the c2d and COMPLETE surveys of Perseus.[4] Perseus is a good test case for such a comparison with a large number of YSOs in different environments from large clusters, such as NGC 1333 and IC 348, to objects in relative isolation or in small groups, such as L1448, L1455, Barnard 1, and Barnard 5. This paper builds on the analysis of Perseus through *Spitzer* (Jørgensen et al. 2006; Rebull et al. 2006) and JCMT SCUBA observations (Kirk et al. 2006) by examining the relation between SCUBA cores and *Spitzer* sources and thereby building a sample of deeply embedded objects. The paper is laid out as follows. Section 2 first examines the general association of mid-infrared sources and the SCUBA cores, the mid-infrared colors of the sources found to be embedded in SCUBA cores (§ 2.1), and the properties of the SCUBA cores with embedded mid-infrared sources (§ 2.2). Section 3 examines the properties of the embedded sources compared to the overall cloud environment in terms of extinction (§ 3.1) and submillimeter flux (§ 3.2). The results of § 2 and § 3 are combined, and an unbiased sample of deeply embedded protostars in Perseus is established. Section 4 presents the sample of sources (§ 4.1) and points to a number of important observational constraints for models of star formation, in particular, in terms of dispersal of newly formed protostars (§ 4.3.1), timescales for the evolution through the prestellar stages (§ 4.3.2), and the star formation efficiency (§ 4.3.3). The results in this paper will also serve as an important pathfinder for comparisons to other clouds surveyed at both mid-infrared and submillimeter wavelengths.

2. MID-INFRARED SOURCES ASSOCIATED WITH DENSE CORES

The first task in building up an unbiased list of embedded YSOs is to define what is meant by an association between a mid-infrared source and a submillimeter core. For this we first explore the distribution of mid-infrared *Spitzer* sources in comparison to the dust condensations seen in the SCUBA maps. In this section we consider the distribution and properties of the nearest MIPS 24 μm source to each submillimeter core and use these to draw general conclusions about the properties of the embedded mid-infrared sources. In § 3.2 we consider the properties of all the MIPS 24 μm sources in the catalog.

Deeply embedded YSOs are expected to have a steeply rising SED from the IRAC through MIPS wavelengths due to the cold envelope emitting at longer wavelengths while absorbing and reprocessing emission from the central star + disk system at shorter wavelengths. We therefore expect any deeply embedded YSO detected at the IRAC wavelengths also to be detected at 24 μm, whereas the inverse may not be true. The Class 0 protostar IRAS 16293−2422 is, for example, seen in IRS observations at 23–35 μm (Jørgensen et al. 2005b; likewise in more sensitive MIPS observations), but not at the IRAC wavelengths. As a first try, we therefore examine the relationship between MIPS 24 μm sources from the c2d observations (Rebull et al. 2006) and the SCUBA cores from the list of Kirk et al. (2006) and H. Kirk et al. (2007, in preparation).[5] The one place where this may be problematic is in regions where the 24 μm maps are confused or bright emission saturates the images. We return to these issues later in this section. Many of the studied sources are also detected at longer wavelengths by MIPS, 70 and 160 μm, where the SED of a typical embedded protostar peaks. On the other hand, these longer wavelength observations are less sensitive, are more likely to be saturated and provide a lower angular resolution, and are therefore less useful for identifying individual objects in an unbiased sense (as is the goal of this paper), especially in confused regions. For establishing the full SEDs of individual objects, these data are important, of course. In the following we refer to the sources detected at 24 μm with MIPS as "MIPS sources."

One concern is how serious the contamination of background sources is and whether these are confused with the YSO population. Based on a comparison to the extragalactic *Spitzer* Wide-Area Infrared Galactic Survey (SWIRE) data, Rebull et al. (2006) find that most of the MIPS sources are background galaxies. Still, the surface density of MIPS sources in the Perseus field is low enough that, given a random spatial distribution, only 0.2 sources would be found within any 1 arcmin^2 or, likewise, that the probability of a chance alignment within 15″ of a given SCUBA core is just a few percent.

Figure 1 shows the distribution of mid-infrared MIPS sources and submillimeter SCUBA cores overlaid on SCUBA maps in a few prominent regions of Perseus. A number of the SCUBA cores are associated with mid-infrared sources within rather small distances. Significant clustering is also seen in other manners, for

---

[4] Throughout this paper we follow the *Spitzer* c2d papers and adopt a distance of 250 pc to Perseus (see discussion in Enoch et al. 2006).

[5] The list of SCUBA cores used in this paper is based on a new processing of the SCUBA maps from Kirk et al. (2006) with smaller (3″) pixel size (H. Kirk et al. 2007, in preparation).
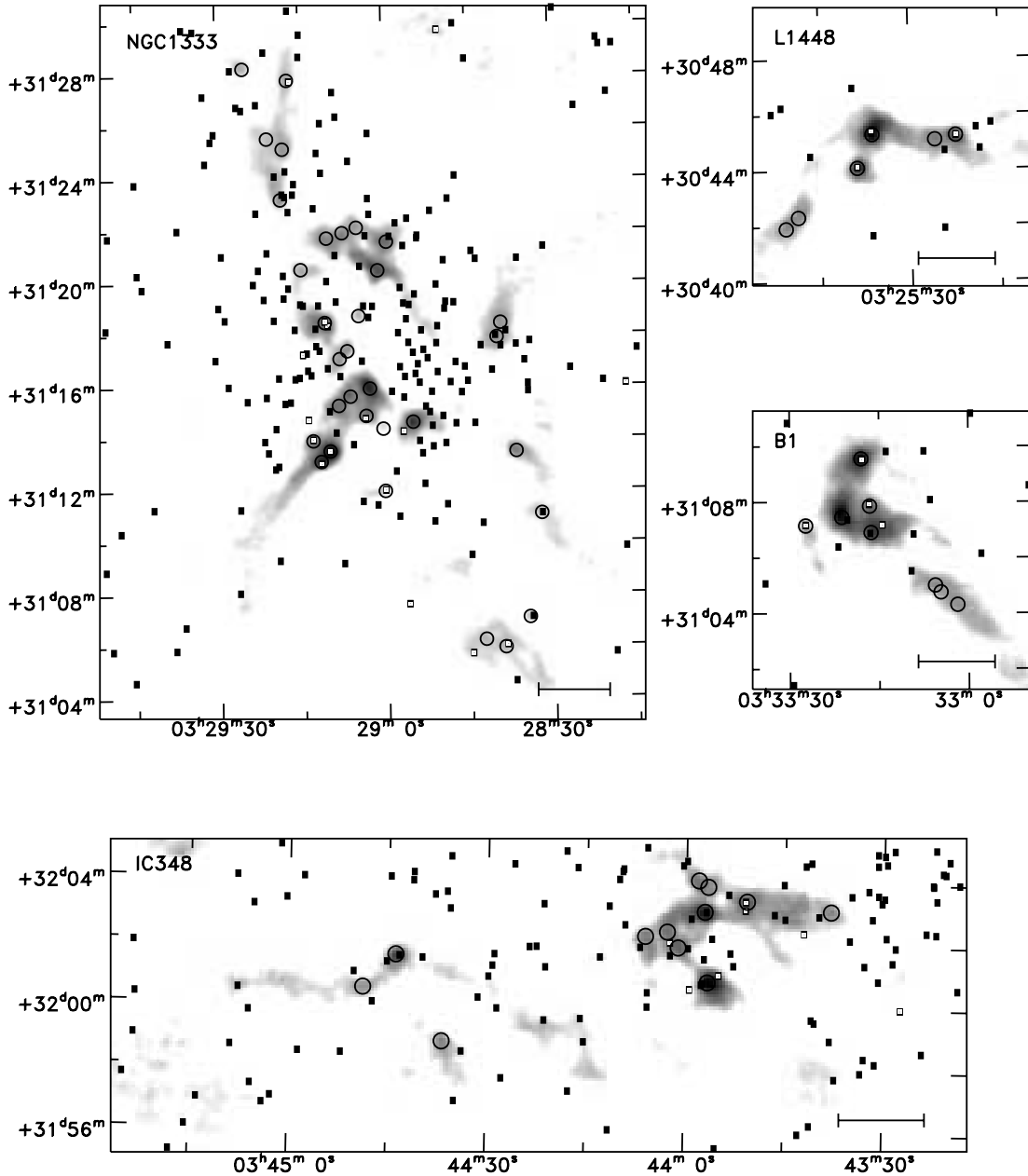
Fɪɢ. 1.—Distribution of SCUBA cores (*circles*) and MIPS sources (*filled squares*), plotted over SCUBA maps of four representative regions of Perseus, from Kirk et al. (2006). The sizes of the symbols of the SCUBA cores correspond to radii of 15″, which is the radius used for determining associations between SCUBA cores and mid-infrared sources. The MIPS sources with $[3.6] − [4.5] > 1.0$ and $[8.0] − [24] > 4.5$ are singled out with open squares. A distance of 0.2 pc is indicated by the scale bar at lower right corner in each panel.

example, the clustering of the submillimeter cores or the mid-infrared sources by themselves. In this paper we only focus on the association of the mid-infrared sources with the submillimeter cores. Of the 72 cores from the SCUBA map, 36 (50%) are found to have a MIPS counterpart within 15″ of the peak (31, or 43%, have a MIPS source within 10″). At the resolution of the *Spitzer* MIPS 24 μm and SCUBA observations (approximately 6″ and 15″, respectively), it appears that most of the SCUBA cores are associated with one MIPS source only (Table 1).

Kirk et al. (2006) defined the radius of each SCUBA core as $R_{obs} = (A/\pi)^{1/2}$, where A is the area of the core at the lowest contour identified by the Clumpfind algorithm (Williams et al. 1994). The typical core radii defined in this way range from approximately 15″ to 45″ (3750–11,250 AU). Figure 2 shows the distribution of MIPS sources around the center of any given core

in units of the radius of each core defined by Kirk et al. (2006), and Figure 3 illustrates the same relationship as a one-dimensional distribution as a function of radius. The red mid-infrared sources are located close to the centers of the submillimeter cores, typically within about 0.5 core radii (significantly more peaked than a random distribution of sources) with a distribution with a full width half-maximum of a few tenths of a core radius (or $\approx 10″$). In § 3.2 we discuss the properties of the red mid-infrared sources with larger separations.

There is a caveat worth mentioning here: is the nearest submillimeter core to each YSO really its parental core? Three effects could come into play: (1) projection effects might play a role, with some SCUBA cores and mid-infrared sources simply being chance alignments; (2) the motion of the YSOs with respect to their surroundings could be significant, making it possible for

TABLE 1
NUMBER OF CORES WITH A GIVEN NUMBER OF (SPECIFIED) SOURCES WITHIN A SPECIFIC RADIUS

| | NUMBER OF SCUBA CORES WITH | | | |
DESCRIPTION	0 Sources	1 Source	2 Sources	3 Sources
MIPS source within 15″	36[a]	33	3	0
MIPS source within 30″	28[a]	34	7	3
"Red"[b] MIPS source within 15″	45	26	1	0
"Red"[b] MIPS source within 30″	42	26	3	1

[a] As discussed in § 2.2, four of these cores are associated with saturated MIPS sources not included in the c2d catalog.
[b] Source with $[3.6] - [4.5] > 1.0$ and $[8.0] - [24] > 4.5$.

sources to travel to the vicinity of different clumps; and (3) the parental core of a given YSO could have been dissipated during the evolution of the YSO. The low surface density of all the MIPS sources argues against the first being a significant effect (see Fig. 2, *bottom*), while the absence of sources with red colors, $[3.6] - [4.5] > 1$, outside the cores and the narrowness of the distribution of their source-core separations argue against the latter two points. In any case, in the above plots (and the discussion in the following sections) each mid-infrared source is only counted once, even though in a few cases a given mid-infrared source is the nearest neighbor to multiple SCUBA cores.

2.1. *Properties of the MIPS Sources*

Not only are the red MIPS sources located close to the center of the submillimeter cores, but an interesting trend is also seen with their colors. It is found that the sources within 1 core radius have red $[3.6] - [4.5] \gtrsim 1$ colors. This is further illustrated in Figure 4, where the colors of the nearest MIPS source to each core have been plotted as a function of distance. In contrast, the $[5.8] - [8.0]$ colors do not show a similar clear trend (Fig. 5). This is consistent with the results of Jørgensen et al. (2006), who showed that the known Class 0 objects in Perseus had very red $[3.6] - [4.5]$ colors, but not similarly red $[5.8] - [8.0]$ colors. The very red $[3.6] - [4.5]$ colors imply that the central protostars are significantly extincted by their ambient envelopes. It is important to note that these objects in fact are detected at such short mid-infrared wavelengths; this is in contrast to the traditional picture of Class 0 objects not being detected at wavelengths shorter than 10 μm. The $[5.8] - [8.0]$ colors in contrast are affected by a number of effects, including absorption in the 10 μm silicate feature, ice absorption, and the intrinsic SED of the central star + disk system (see also discussion in Jørgensen et al. 2006). The $[8.0] - [24]$ color also shows an increase at small source-core separations (Fig. 6), and only a few MIPS sources with $[8.0] - [24] \gtrsim 4.5$ have distances larger than 15″. In contrast to the comparison with the $[3.6] - [4.5]$ colors, the trend is not unambiguous; some objects are found with small distances and $[8.0] - [24] \lesssim 4.5$. This is similar to what was observed by Muzerolle et al. (2004), who found that objects of differing embeddedness (Class 0–II) showed some overlap in their $[8.0] - [24]$ colors. One source (IRAS 03256+3055) has both very red $[3.6] - [4.5]$ and $[8.0] - [24]$ colors and is standing out a distance of about 43″ to the nearest submillimeter core; inspection of the submillimeter maps reveals clear extended dust continuum emission at this position, which, due to confusion, is not identified as a core. Another red MIPS source with a large separation of 31″ is seen from visual inspection of the IRAC and MIPS images to be located close to the L1448-IRS 2 Outflow. This MIPS source is likely to be a chance alignment, and its red $[3.6] - [4.5]$ colors just a result of (unrelated)

shocked H$_2$ emission in the L1448–IRS 2 outflow showing up prominently at 4.5 μm. This source is excluded from the sample in the following discussions.

Each source in the c2d catalogs is classified with the aim of separating stars, YSO candidates, and other sources (mainly background galaxies) according to cuts in the IRAC and MIPS color planes (Evans et al. 2005). In this way, Jørgensen et al. (2006) identified 400 candidate YSOs in the 3.86 deg^2 of Perseus covered by the IRAC observations. Not all the 39 MIPS sources (within 15″ of one of the 36 submillimeter cores with embedded YSOs) were included in that list, however. As a first cut, the high-quality catalog used in Jørgensen et al. (2006) excluded all sources that appear extended in one or more IRAC bands, as such sources have less reliable photometry. As discussed in Jørgensen et al., this is an issue for the embedded YSOs in particular, since they often appear extended in one or more of the IRAC images, either due to H$_2$ emission from shocks in the outflows or scattered light at the IRAC wavelengths. Of the 39 MIPS sources discussed above, 18 show extended emission and are excluded from the list of objects studied by Jørgensen et al.

In addition, the classification of YSOs described in Evans et al. (2005) relies on detection in at least three bands (of the four IRAC bands and MIPS 24 μm), and very deeply embedded YSOs may therefore not be picked out by these criteria if, for example, they are too faint at the shortest IRAC wavelengths. Of the 39 MIPS sources discussed above, 29 (74%) were classified as YSOs based on their colors. Of the remaining objects, two are only detected at 24 μm, but not the shorter IRAC wavelengths, while the remaining eight are found to have red SEDs (3 times stronger MIPS flux than flux at the nearest IRAC wavelength), but do not meet the YSO criteria used by Jørgensen et al. (2006). Of the 29 MIPS sources that are candidate YSOs based on their colors, 17 show extended emission in one or more IRAC bands, and only the remaining 12 are therefore included in the sample of YSOs in Jørgensen et al. (2006). In summary, the embedded YSOs from this paper should be added to the general list of YSOs in Perseus from Jørgensen et al.; about two out of three of the embedded YSOs did not make it onto that list.

2.2. *Properties of the Cores*

It is interesting to investigate whether the submillimeter cores with embedded red sources have distinct properties compared to those without, in particular, to distinguish the starless from the star-forming cores based on the submillimeter maps by themselves. A promising empirical characteristic of cores appears to be their concentration,

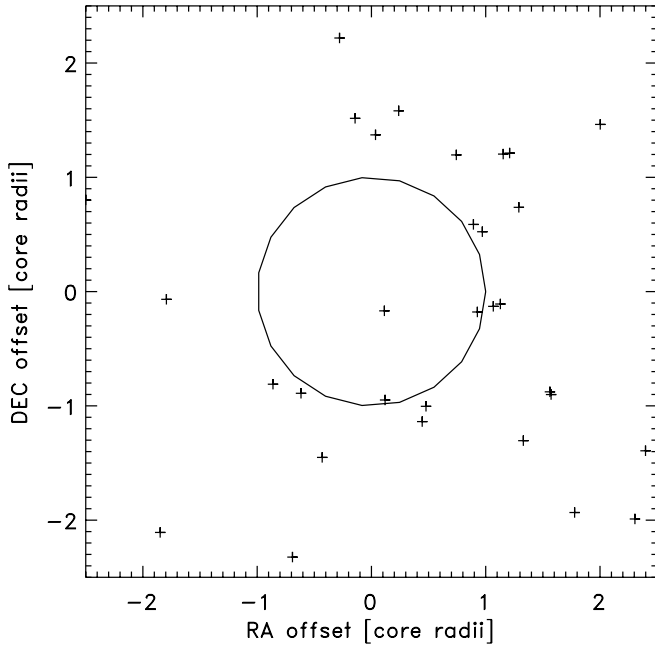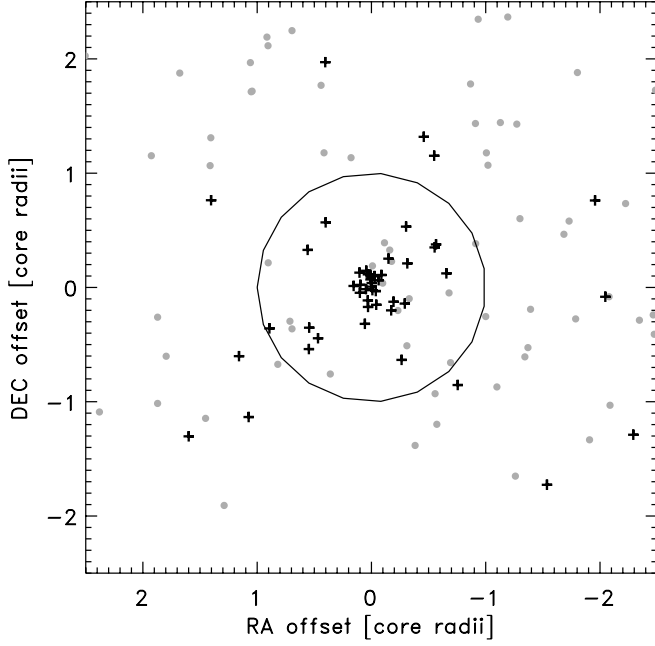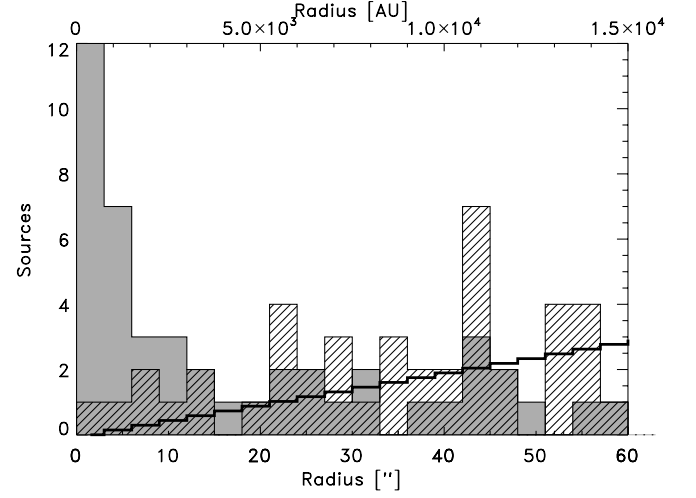$$C = 1 - \frac{1.13B^2 S_{850}}{\pi R_{\rm obs}^2 f_0}, \qquad (1)$$

Fig. 3.—Distribution of the number of mid-infrared sources as a function of distance. The shaded gray histogram indicates the distribution of sources with $[3.6] - [4.5] \geq 1.0$, and the hatched histogram the distribution of sources with $[3.6] - [4.5] < 1.0$. The thick black line indicates the prediction from a uniform source distribution with the same surface density as the observed distribution.

Fig. 2.—*Top*: Distribution of MIPS sources with IRAC detections around the center of the nearest SCUBA core (all shifted to a common center) for any given MIPS source. The distances are given in units of the core radii. Sources with $[3.6] - [4.5] \geq 1.0$ are shown with black plus signs, and sources with $[3.6] - [4.5] < 1.0$ are shown with gray dots. *Bottom*: For comparison, the similar plot for a random distribution of the MIPS sources over the SCUBA field.

where B is the beam size, S_{850} is the total flux from the SCUBA observations at 850 μm, $R_{\rm obs}$ is the measured radius, and f_0 is the peak flux. From comparison between SCUBA maps and optical and near-infrared images of shocks in the Barnard 1 region, Walawender et al. (2005) found that all the SCUBA cores with concentrations >0.75 contained protostars with a decreasing fraction with lower concentrations and that none of the cores with concentrations <0.4 had embedded protostars. Walawender et al. (2006) and Johnstone & Bally (2006) have extended this reasoning to IC 348 and Orion A South, respectively. Figures 7 and 8 compare the number of cores with a given concentration
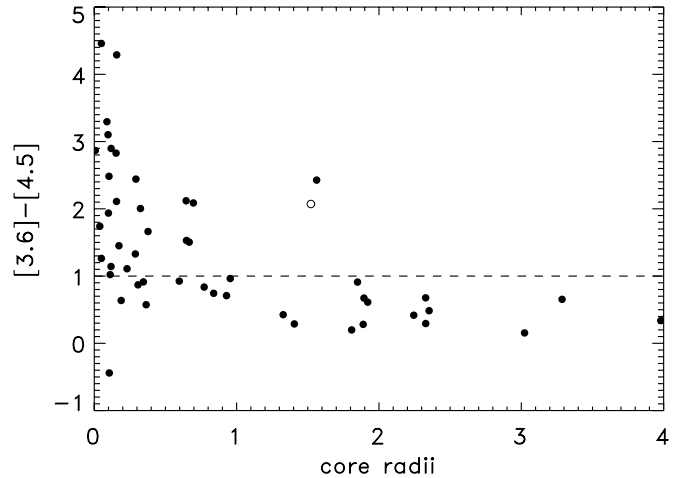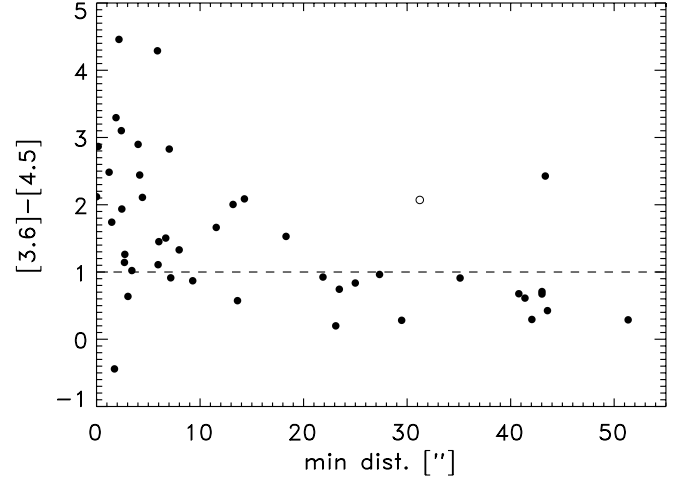

Fig. 4.—Nearest MIPS detection to each core and its $[3.6] - [4.5]$ color vs. distance in arcseconds (*top*) and core radii (*bottom*). The shock associated with the L1448–IRS 2 outflow is indicated by an open symbol.
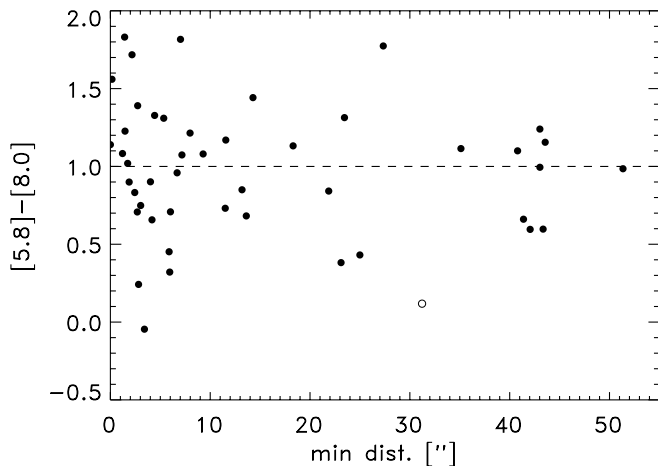
FIG. 5.—Nearest MIPS detection to each core and its [5.8] − [8.0] color vs. distance.

FIG. 7.—Distribution of "concentrations" of SCUBA cores. Those with embedded YSOs within 15″ are doubly hatched, while the additional four cores with concentrations higher than 0.6 discussed in the text are singly hatched.

and total 850 μm flux with embedded YSOs to the total number of cores. There is a trend in that most cores with concentrations higher than 0.6 have embedded YSOs. A number of effects could cause this empirical distinction. As the concentration is a measure of the brightness distribution of the submillimeter emission, it will be affected by the formation of a central protostar; i.e., an object with an internal source of heating will show more emission toward the center and therefore appear more concentrated. Also, when considering only prestellar cores, under the above definition Bonnor-Ebert spheres stable against collapse have $C < 0.72$ (Johnstone et al. 2000), whereas cores with higher concentrations are either collapsing or require support from other mechanisms (e.g., magnetic fields) in addition to the thermal support. Still, even a highly condensed prestellar core such as L1544 (e.g., Evans et al. 2001; Crapsi et al. 2005) has a concentration of ≈0.5 estimated from SCUBA maps of the core and would therefore not fall into the above group of objects.

There also seems to be a distinction between the SCUBA cores with and without embedded YSOs in terms of their total submillimeter flux. We find that 80% of the starless cores have fluxes lower than 2 Jy (see also Table 2), although the trend is not as clear-cut as for the concentrations. As for the concentrations, it is interesting to note that a number of the cores with embedded
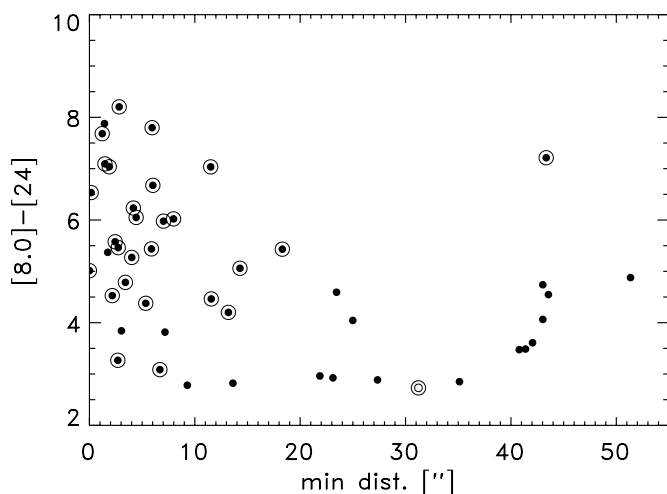
YSOs do have low fluxes. If the cores all had the same dust temperatures, the trend would imply an evolution with core mass. In cores with embedded YSOs, the dust temperature will be higher due to the heating by the central protostar, and the mass lower than the mass of a comparable starless core with similar flux. Since most starless cores have fluxes lower than 2–3 Jy (or masses lower than 1–1.5 $M_\odot$), this is not a significant effect. No clear trend in any of these parameters is seen for the cores with multiple embedded mid-infrared sources (Table 1), compared to the overall sample of cores with only one embedded source.

Four SCUBA cores with concentrations larger than 0.6 do not have any embedded MIPS sources from the criteria above. One example is NGC 1333–IRAS 2A, a well-studied Class 0 protostar that is clearly identified, but saturated, in the MIPS 24 μm images. At the IRAC wavelengths extended emission from its jet is seen, causing its photometry to be unreliable, similar to the problems of other Class 0 objects (Jørgensen et al. 2006). Furthermore, its companion NGC 1333–IRAS 2B (separation of 30″) is clearly identified as a YSO at all four IRAC bands and MIPS, but its SCUBA flux is dominated by the emission from IRAS 2A. Similar issues are also seen for the remaining SCUBA cores with high concentrations, which are associated with the previously known infrared sources, IRAS 03255+3103, NGC

FIG. 6.—Nearest MIPS detection to each core and its [8.0] − [24] color vs. distance. Sources with [3.6] − [4.5] > 1 are indicated with an additional outer circle around their symbol.
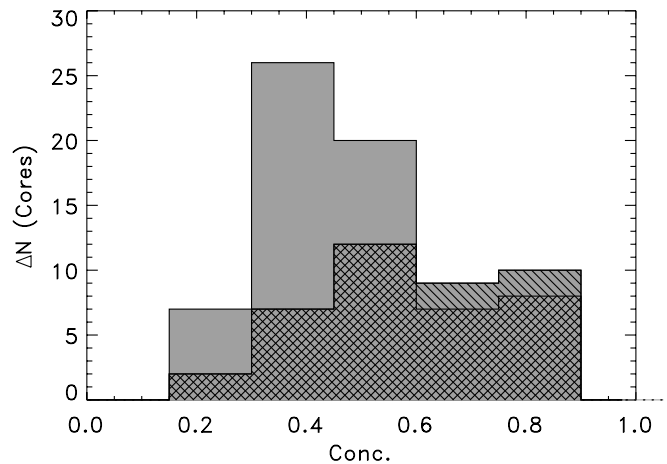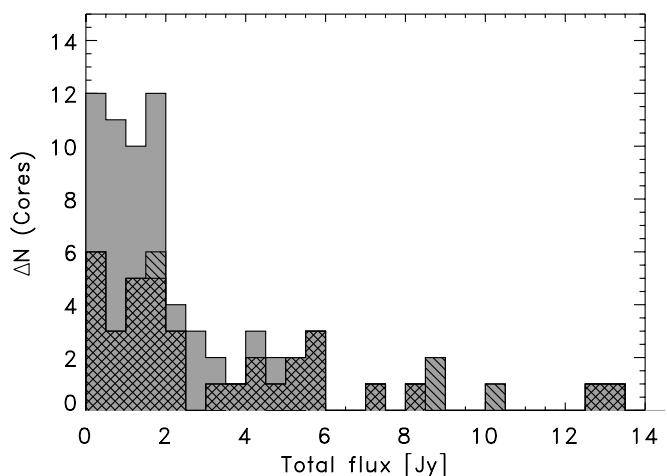

FIG. 8.—Same as Fig. 7, but for the distribution of total 850 μm fluxes of the SCUBA cores.

TABLE 2
NUMBER OF CORES WITH AND WITHOUT EMBEDDED YSOs AS A FUNCTION OF CORE FLUX

Total 850 μm Flux Range (Jy)	Total	With Embedded YSOs (%)	Percent with Embedded YSOs	Mass Range[a] ($M_{\odot}$)
<0.5	12	6	50	<0.25
0.5–1	12	3	25	0.25–0.5
1–2	21	11	52	0.5–1.0
2–4	10	5	50	1.0–2.0
4–6	10	8	80	2.0–3.0
>6	7	7	100	>3.0

[a] Assuming a dust temperature of 15 K and a dust opacity of 0.0182 cm^2 g^{-1} at 850 μm.

1333–SVS 12, and NGC 1333–SVS 13. None of the remaining starless cores (i.e., cores with no associated mid-infrared sources) with concentrations less than 0.6 are found to have embedded YSOs from visual inspection of the MIPS and IRAC images.

Again, this poses the problem of whether there are more sources with IRAC detections and red colors but no MIPS detections. Besides the saturation issue of MIPS, this could also be the case in regions where the sources are confused at the slightly poorer MIPS resolution. Only seven red sources are found with $[3.6] - [4.5]$ colors greater than 1.0 and no MIPS counterpart. These include the sources in the cores discussed above, a shock knot associated with the NGC 1333–IRAS 4A outflow, three fainter companions to strong MIPS sources, and a faint (mJy level) IRAC source in a dust condensation southeast of L1448. So, generally, it appears that the MIPS detection requirement is useful to identify embedded YSOs, although confusion might arise in regions with many bright MIPS sources.

In summary, the submillimeter cores with concentrations higher than 0.6 are all star-forming, with a decreasing trend toward lower concentrations, but it is worth noting that a number of low-concentration/flux cores do have embedded YSOs, so this distinction is not unique. In § 4.1 we use these results, together with the results concerning the spatial distribution of embedded YSOs and their colors from the above discussions, to establish an unbiased list of embedded YSOs.

3. COMPARISON TO THE OVERALL CLOUD ENVIRONMENT

3.1. *Extinction as a Tracer*

The submillimeter cores are in general found in regions of high extinction (Enoch et al. 2006; Kirk et al. 2006), suggesting an extinction threshold for the formation of the dust cores (see also Johnstone et al. 2004). A similar trend is seen when comparing the location of the mid-infrared sources to the extinction maps from COMPLETE (J. Alves & M. Lombardi 2007, in preparation; Kirk et al. 2006). Figure 9 shows the cumulative distribution of red MIPS sources as a function of A_V. From this figure it is found that 90% of the YSOs with $[3.6] - [4.5] > 2$ are at $A_V > 5$, which is similar to the extinction threshold for the cores in Perseus (Enoch et al. 2006; Kirk et al. 2006), as one would expect from the relation between the dense cores and the embedded YSOs. This, of course, also begs the question of whether the observed trends in colors simply reflect the overall cloud extinction toward the low-mass protostars. It is unlikely, since even a fairly high amount of extinction only produces a small shift in $[3.6] - [4.5]$ colors; according to the extinction measurements of T. Huard et al. (2007, in preparation), for an $A_V = 50$ ($A_K = 5.6$) a shift of $E_{[3.6]-[4.5]} = 0.36$ is expected. This is also similar to the conclusion of studies examining the

properties of YSOs in color-color diagrams (e.g., Allen et al. 2004), which generally find that the YSOs have infrared excesses that cannot be explained by extinction from the cloud material, but rather are due to a combination of the extinction in the inner parts of the protostellar envelopes and emission from warm dust in the envelope and disk.

3.2. *Submillimeter Flux as a Tracer*

The discussion in § 2 was based on the question, What is the nearest MIPS source to any given SCUBA core? To fully address the completeness of this method, we also have to ask the inverse question, What is the distance for any given red source to its nearest submillimeter core? Figures 10 and 11 show the $[3.6] - [4.5]$ and $[5.8] - [8.0]$ colors of all the MIPS sources as a function of distance to the nearest SCUBA core. In both Figures 10 and 11, a number of red sources are found with distances of $20'' - 100''$ to their nearest cores. This does not mean that these red objects are not associated with high levels of extinction. Figure 12 shows the cumulative distribution of SCUBA fluxes at the positions of YSOs with $[3.6] - [4.5]$ colors lower than 1, between 1 and 2, and higher than 2. The reddest objects ($[3.6] - [4.5] > 2$) are found in regions with SCUBA fluxes higher than 0.1 Jy beam^{-1} (90% of the red sources), corresponding to an extinction $A_V \gtrsim 7$ for a dust temperature of 15 K and an 850 μm dust opacity per unit total (dust + gas) mass of 0.0182 cm^2 g^{-1} (Ossenkopf & Henning 1994). In effect, the amount of extinction

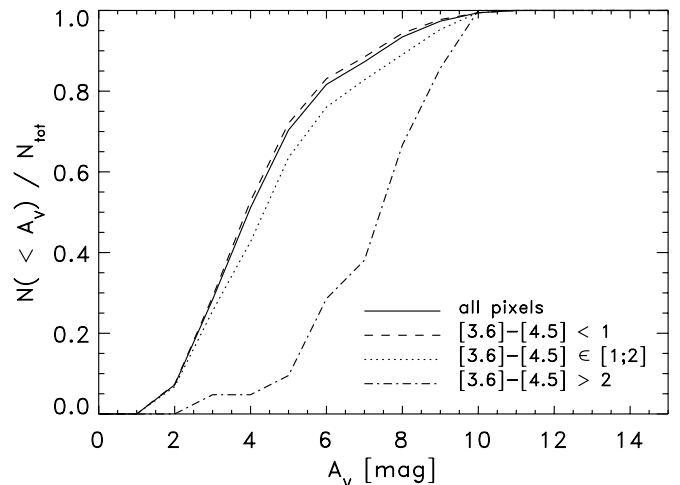FIG. 9.—Cumulative fraction of mid-infrared sources with differing $[3.6] - [4.5]$ colors as a function of A_V from the extinction maps. The four different lines indicate all the pixels from the extinction map covered by the mid-infrared observations (*black solid line*) and mid-infrared sources with $[3.6] - [4.5] < 1$ (*dashed line*), $1 \leq [3.6] - [4.5] \leq 2$ (*dotted line*), and $[3.6] - [4.5] > 2$ (*dash-dotted line*).
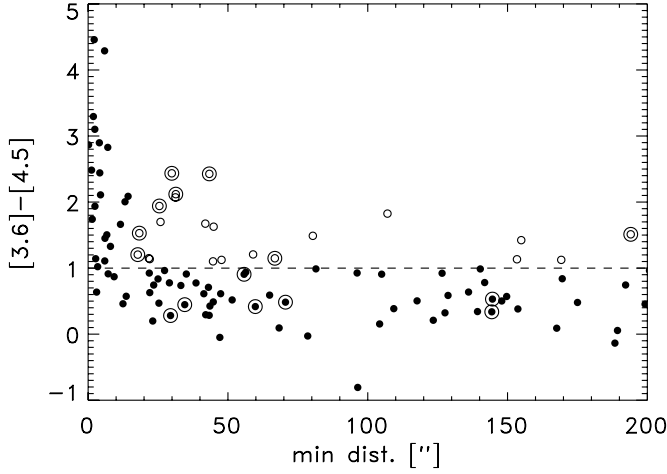
FIG. 10.—The [3.6] − [4.5] color of each MIPS source vs. its distance to the nearest submillimeter core. Sources with distances larger than 15″ to their nearest submillimeter core and [3.6] − [4.5] > 1.0 are indicated by open circles. A second larger circle around any symbol (*filled or open circle*) indicates a mid-infrared source with a distance to the nearest submillimeter core larger than 15″ and with a [8.0] − [24] color greater than 4.5 (those sources are also indicated by open circles in Fig. 11).

will be lower for protostars that are heating their envelopes to higher temperatures, but, on the other hand, since high amounts of extinction are required to explain the very red colors, the actual central extinction is significantly higher than that calculated on the basis of the SCUBA flux due to beam dilution. It should also be contrasted with the average extinction from the extinction maps (§ 3.1), which measures the larger scale structure of the cloud.

Visual inspection of the SCUBA data at the positions of the MIPS sources with distances to their nearest core larger than 15″, [3.6] − [4.5] > 1.0, and [8.0] − [24] > 4.5 reveals that almost all of these are associated with dust continuum peaks with low fluxes. This demonstrates that in the confused regions, in particular, the exact identification of cores is somewhat dependent on the algorithm, assumed noise level, etc., as demonstrated by a comparison between the lists of cores in Perseus from Kirk et al.
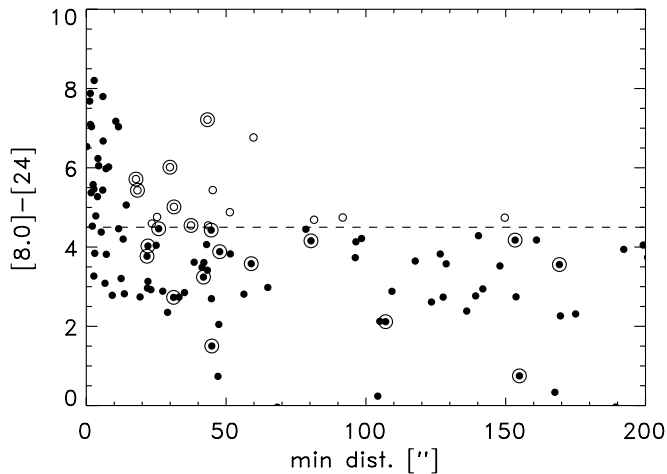

FIG. 11.—The [8.0] − [24] color of each MIPS source vs. its distance to the nearest submillimeter core. Sources with distances larger than 15″ to their nearest submillimeter core and [8.0] − [24] > 4.5 are indicated by open circles. A second, larger circle around any symbol (*filled or open circle*) indicates a mid-infrared source with a distance to the nearest submillimeter core larger than 15″ and with a [3.6] − [4.5] color greater than 1.0 (those sources are also indicated by open circles in Fig. 10).
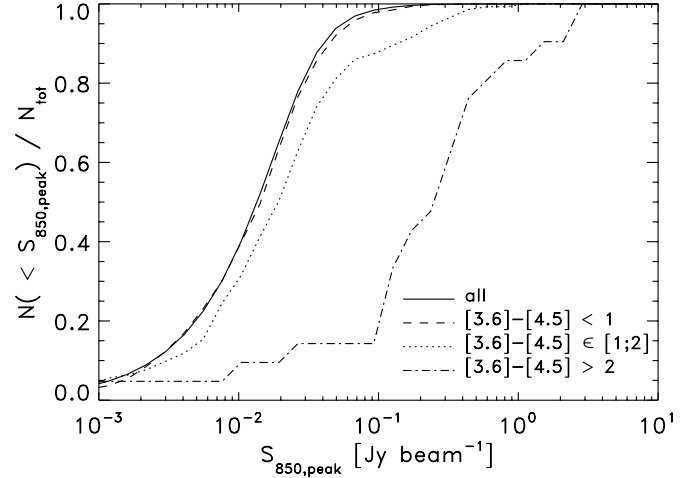

FIG. 12.—Cumulative number of mid-infrared sources (with signal-to-noise ratio (S/N) of 7 or greater in IRAC bands 1 and 2) as a function of SCUBA flux at the position of the MIPS source, divided according to [3.6] − [4.5] colors as in Fig. 9.

(2006) and Hatchell et al. (2005) (both based on similar, but not identical, SCUBA 850 μm data, but processed differently) and that of Enoch et al. (2006), based on Bolocam 1.1 mm data (see also the discussion in Young et al. 2006). Still, by imposing the color criteria above, it is possible to pick out the remaining YSO candidates that are missed for lack of a core extracted from the submillimeter maps for those reasons.

4. DISCUSSION

4.1. *Constructing an Unbiased Sample of Embedded YSOs*

Based on the above discussions, it is possible to create a relatively unbiased list of 49 deeply embedded YSOs in Perseus (Table 3) by selecting sources that meet any of the following three criteria:

1. MIPS catalog sources with [3.6] − [4.5] > 1 and [8.0] − [24] > 4.5 (23 sources);
2. MIPS catalog sources with distances less than 15″ to their nearest core (39 sources);
3. submillimeter cores with concentrations higher than 0.6 (21 sources).

The first criterion will select all MIPS sources that are embedded YSOs, but miss sources that are not detected in IRAC bands 1 or 2, either due to confusion with outflows or simply because they in fact are very deeply embedded. That list will also include sources that are not necessarily directly associated with a submillimeter core due to confusion in the submillimeter map, poorly defined cores, or simply the sensitivity of the submillimeter observations. The second criterion will select the most deeply embedded YSOs with steeply increasing SEDs, such as IRAS 16293−2422 (Jørgensen et al. 2005b). As pointed out in § 2.1, most of the sources selected by these first two criteria will be overlapping, but sources that are saturated at 24 μm will be missed. Such sources will be selected by criterion (3), which does not include all the mid-infrared sources under (1) and (2), as shown in Figure 7. Neither the mid-infrared source lists nor the submillimeter core identifications by themselves can be used unambiguously to define a sample of embedded objects. Applying, for example, only criterion 1, which is based solely on the mid-infrared colors, or criterion 3, which is based solely on the submillimeter maps, would pick out only 40%–50% of the sources, but used in

TABLE 3
LIST OF EMBEDDED YSOs IN PERSEUS

Number	Position[a] R.A. (J2000.0)	Decl. (J2000.0)	Mid-IR Colors [3.6] − [4.5]	[8.0] − [24]	Separation[b] (arcsec)	Concentration[c]	Code[d]	Other Identifiers[e]	Reference
1..............	03 25 22.36	+30 45 13.6	2.9	6.5	0.2	0.70	ABC	L1448−IRS 2/IRAS 03222+3034	
2..............	03 25 36.48	+30 45 23.2	2.8	6.0	7.0	0.87	ABC*	L1448-N(A)	
3..............	03 25 38.87	+30 44 06.0	1.7	7.1	1.5	0.83	ABC	L1448-C(N)	
4..............	03 26 37.46	+30 15 28.2	2.4	6.2	4.2	0.39	AB−	. . .	
5..............	03 27 38.27	+30 13 58.5	0.6	3.8	3.0	0.31	−B−*	L1455-FIR2	1
6..............	03 27 39.11	+30 13 02.8	3.3	7.0	1.9	0.59	AB−*	L1455−IRS 1/IRAS 03245+3002	
7..............	03 27 43.25	+30 12 28.9	2.1	6.1	4.4	0.57	AB−	L1455−IRS 4	
8..............	03 27 47.69	+30 12 04.4	0.9	2.8	9.3	0.48	−B−*	. . .	
9..............	03 28 32.55	+31 11 04.8	−0.4	5.4	1.7	0.27	−B−	. . .	
10..............	03 28 34.53	+31 07 05.5	1.5	3.1	6.7	0.30	−B−*	. . .	
11..............	03 28 37.11	+31 13 28.3	2.8	. . .	. . .	0.66	−−C	IRAS 03255+3103	
12..............	03 28 39.11	+31 06 01.6	1.3	6.0	8.0	0.32	AB−	(ass. HH 340)	
13..............	03 28 40.62	+31 17 56.5	. . .	4.4	5.3	0.51	−B−	. . .	
14..............	03 28 45.31	+31 05 41.9	2.4	7.2	43.3	. . .	A−−	IRAS 03256+3055	
15..............	03 28 55.59	+31 14 37.5	. . .	. . .	. . .	0.87	−−C	NGC 1333−IRAS 2A	
16..............	03 28 57.36	+31 14 15.9	2.1	5.0	31.4	. . .	A−−*	NGC 1333−IRSA 2B	
17..............	03 28 59.55	+31 21 46.7	0.6	2.8	13.6	0.67	−BC*	. . .	
18..............	03 29 00.61	+31 12 00.4	. . .	. . .	2.4	0.48	−B−	. . .	
19..............	03 29 01.66	+31 20 28.5	. . .	. . .	. . .	0.67	−−C	(ass. SVS 12/ASR 114)	
20..............	03 29 03.30	+31 15 55.5	. . .	. . .	. . .	0.77	−−C	NGC 1333−SVS 13	
21..............	03 29 04.09	+31 14 46.6	1.5	6.7	6.0	0.53	AB−	HH 7−11 MMS6	
22..............	03 29 10.53	+31 13 30.7	. . .	. . .	0.8	0.86	−BC	NGC 1333−IRA S4A	
23..............	03 29 10.72	+31 18 20.5	. . .	7.2	10.6	0.74	−BC2	. . .	
24..............	03 29 11.29	+31 18 31.3	. . .	8.2	2.8	0.74	−BC2	. . .	
25..............	03 29 12.07	+31 13 01.8	4.3	5.4	5.9	0.86	ABC	NGC 1333−IRAS 4B[f]	
26..............	03 29 13.62	+31 13 57.9	3.1	. . .	2.4	0.58	−B−	NGC 1333−IRAS 4C	
27..............	03 29 17.21	+31 27 46.2	1.1	7.8	5.9	0.54	AB−	(ass. Per 4)	2
28..............	03 29 18.25	+31 23 19.9	1.7	4.5	11.6	0.55	−B−*2	(ass. HH 335)	
29..............	03 29 18.73	+31 23 25.4	0.5	3.2	12.5	0.55	−B−*2	. . .	
30..............	03 29 23.50	+31 33 29.4	. . .	7.0	11.5	0.43	−B−	IRAS 03262+3123	
31..............	03 29 51.89	+31 39 05.6	. . .	7.9	1.4	0.53	−B−	IRAS 03267+3128/(Per 5)	2
32..............	03 31 21.01	+30 45 30.0	1.9	5.6	2.4	0.71	ABC	IRAS 03282+3035	
33..............	03 32 18.03	+30 49 46.9	1.0	4.8	3.4	0.82	ABC	IRAS 03292+3039	
34..............	03 33 13.81	+31 20 05.2	2.1	5.1	14.3	0.31	AB−	(ass.Per 9B)	2
35..............	03 33 14.41	+31 07 10.8	2.4	6.0	29.9	. . .	A−−*2	B1-SMM3	
36..............	03 33 16.49	+31 06 52.3	. . .	. . .	2.7	0.55	−B−2	B1-d	
37..............	03 33 16.67	+31 07 55.1	2.9	5.3	4.0	0.38	AB−	B1-a/IRAS 03301+3057	
38..............	03 33 17.87	+31 09 31.8	4.5	4.5	2.2	0.84	ABC*	B1-c	
39..............	03 33 20.34	+31 07 21.4	2.0	4.2	13.2	0.74	−BC*	B1-b	
40..............	03 33 27.31	+31 07 10.2	2.5	7.7	1.2	0.32	AB−	(ass. HH 789)	
41..............	03 43 50.99	+32 03 24.7	1.3	5.5	2.7	0.65	ABC	. . .	
42..............	03 43 51.03	+32 03 08.0	1.2	5.7	17.8	. . .	A−−*	. . .	
43..............	03 43 56.91	+32 03 04.2	. . .	. . .	3.1	0.79	−BC	IC 348−MMS	
44..............	03 43 57.32	+32 00 47.6	. . .	. . .	8.3	0.78	−BC2	HH 211−FIR (?)	
45..............	03 43 57.64	+32 00 44.8	. . .	. . .	13.1	0.78	−BC2	(ass. HH 211?)	
46..............	03 43 59.41	+32 00 35.5	2.6	4.5	37.5	. . .	A−−	(ass. HH 211?)	
47..............	03 44 02.40	+32 02 04.7	1.5	5.4	18.3	. . .	A−−	. . .	
48..............	03 44 43.32	+32 01 31.6	0.9	3.8	7.2	0.62	−BC*	IRAS 03415+3152	
49..............	03 47 41.61	+32 51 43.9	1.1	3.3	2.7	0.59	−B−*	B5−IRS 1/IRAS 03445+3242	

NOTE.—Units of right ascension are hours, minutes, and seconds, and units of declination are degrees, arcminutes, and arcseconds.

[a] Coordinates for sources selected on the basis of the core concentration only (code C) refer to the position of the SCUBA core.

[b] Separation between the mid-infrared source and the nearest submillimeter core.

[c] Concentration of submillimeter core from Kirk et al. (2006).

[d] Code for selection of source according to which of the criteria (A, B, or C) in § 4.1 applies for the given source. Sources included in the list of Jørgensen et al. (2006) are furthermore identified by asterisks. Cores associated with multiple YSOs (within 15″) in Table 1 are furthermore identified by a 2 in this code.

[e] Refers to main designation in the SIMBAD database, commonly used identifier or association (marked "ass.").

[f] The c2d catalog refers to the position of bright shock observed in the IRAC bands.

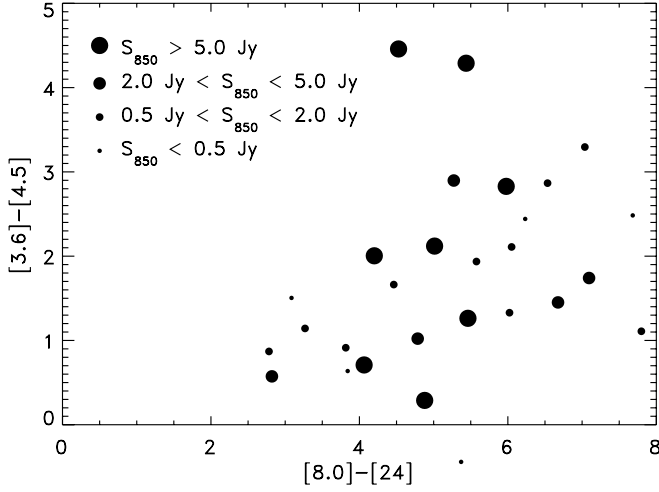REFERENCES.—(1) Tapia et al. 1997; (2) Ladd et al. 1994.

FIG. 13.—The [3.6] − [4.5] vs. [8.0] − [24] color-color diagrams for the embedded YSOs. For each YSO the size of the symbol indicates the total flux of the parental core from the submillimeter observations (Kirk et al. 2006).

conjunction they will form a relatively unbiased list of YSOs, complete down to the resolution of the mid-infrared data. It should also be emphasized that these YSOs constitute an important addition of embedded sources to the list of YSOs discussed in Jørgensen et al. (2006), although they only constitute a small fraction (≈10%) of the overall YSO population in the cloud.

4.2. Colors of Deeply Embedded Protostars

It is interesting to examine whether there is any evolution of the colors of the embedded YSOs compared to the properties of their parental cores. For example, do the more massive cores generally have more deeply embedded protostars with redder mid-infrared colors? As shown in Figure 8, cores with stronger submillimeter fluxes all have embedded sources, but a significant number of "fainter" cores also appear to be forming stars.

Figure 13 shows the [3.6] − [4.5] and [8.0] − [24] colors of the embedded YSOs with the fluxes of their parental cores indicated. There are two interesting effects to note. (1) This diagram includes all the MIPS sources located within 15″ of a submillimeter core, and for those sources there is a clear trend across the diagram, with an increase in both colors (from zero or no infrared excess) toward higher values, possibly approaching a maximum value of their [8.0] − [24] colors of about 6–8. (2) If we apply our criterion of [3.6] − [4.5] > 1 for embeddedness, the [8.0] − [24] colors do not actually increase systematically with flux, but are rather scattered around a value of about 6. Some of the brighter SCUBA cores have YSOs with very red colors, but note also that some mid-infrared sources associated with fairly bright cores have [3.6] − [4.5] ≲ 1.0.

The upturn in colors is roughly as predicted by the models of Whitney et al. (2003), but this diagram extends to much bluer [8.0]−[24] colors than predicted in their models. On the other hand, the [3.6] − [4.5] colors are much redder than predicted from the models. Whitney et al. (2003) find that only a few deeply embedded YSOs should be detectable at the shortest. IRAC wavelengths. That we actually detect a significant fraction of the deeply embedded protostars might again reflect that the envelopes have larger cleared-out cavities, similar to the case of IRAS 16293−2422A (Jørgensen et al. 2005b), in contrast to the assumption of the models of Whitney et al. (2003), which extend to 7 stellar radii. At such small inner radii, the mid-infrared emis-

sion from the central protostar would be completely absorbed by the surrounding envelope, and the object would not be detectable at the IRAC wavelengths. The fact that most of these sources are detectable at 3.6 and 4.5 μm suggests that this is not the case and that the [3.6] − [4.5] color therefore is a potentially interesting diagnostic of the properties of the disks and inner envelopes of deeply embedded protostars.

4.3. Constraints on Star Formation

As pointed out in the introduction, many important constraints on low-mass star formation hinge on statistical arguments, such as using the relative number of pre- and protostellar cores to estimate their lifetimes. Previous studies have often been based on compilations of different surveys that were not necessarily observed under similar conditions or with the same techniques and have often required the combination of data for many clouds to obtain statistically meaningful samples. The strength of the combination of the *Spitzer* and SCUBA data presented in this paper is that it represents a relatively uniform survey of just one cloud and still has enough cores and protostars that strong statements can be made without many of the caveats introduced otherwise. We here discuss the constraints on three important aspects of low-mass star formation introduced by this study.

4.3.1. Motions and Dispersal of Protostars

One of the debated issues in current theories of star formation is the importance of the motions of embedded YSOs through the medium for their accretion rates, i.e., basically whether Bondi-Hoyle accretion (Bondi & Hoyle 1944) applies. The simulations of Bonnell et al. (1997, 2001) and Bate et al. (2003), for example, show that the motions of the embedded YSOs through their ambient medium will have a significant impact on their accretion histories and thereby on the resulting distribution of YSOs as a function of mass. On the other hand, based on a study of locations of YSOs in different evolutionary stages from Taurus, Hartmann (2002) argues that the velocity dispersion of the YSOs once formed is small, ≲0.2 km s^{-1}. The narrowness of the distribution of separations between the mid-infrared sources and submillimeter cores (Fig. 3) indicates that the dispersal of newly formed stars in Perseus is similar to that in Taurus.

As shown in Figure 3, typical separations between the mid-infrared sources and submillimeter cores are less than $l \approx 10″$. Assuming a typical lifetime of the deeply embedded protostars of $t = 10^5$ yr, the velocity dispersion is

$$\delta v = \frac{l}{t} = 0.1 \text{ km s}^{-1} \left(\frac{l}{10″} \right) \left(\frac{d}{250 \text{ pc}} \right) \left(\frac{t}{10^5 \text{ yr}} \right)^{-1}, \quad (2)$$

which is smaller than the isothermal sound speed, $c_s = (kT/m)^{1/2} \approx$ 0.2 km s^{-1} for a molecular cloud with a temperature of 10–15 K. Walsh et al. (2004) examined the motions of dense cores traced by N$_2$H$^+$ $J = 1–0$ emission with respect to less dense ambient envelopes traced by ^{13}CO and C^{18}O $J = 1–0$. They found only small velocity differences between the "cores" and "envelopes," which they took as evidence that dense cores did not have significant velocities with respect to their surroundings. Ayliffe et al. (2007) examined the models of Bate et al. (2003) using an approach similar to that in Walsh et al. (2004) and also found small velocities of the cores relative to their lower density ambient envelopes. It therefore appears that those simulations are not invalidated by the observations of Walsh et al. What is shown by this analysis, however, is that the newly formed stars still embedded within their parental cores also do not have highly supersonic

velocities and therefore do not seem to travel a substantial distance during their main accretion phase. It is also interesting to note the similarity to Taurus; even though Taurus is thought to be forming low-mass stars in a more quiescent fashion compared to Perseus, the velocity dispersions are very similar and significantly below the 1 km s^{-1} virial speeds inferred from models of protostars accreting while moving through the molecular cloud (and halting accretion when "leaving" the densest regions).

4.3.2. Timescales

This study finds that approximately half the SCUBA cores from the study of Kirk et al. (2006) have embedded YSOs. This suggests that the dissipation timescale of the cores once a protostar has been formed is similar to the timescale during which the cores evolve through the part of the prestellar stage observable by the SCUBA studies. Lee & Myers (1999) studied a sample of optically identified cores and found that only 24% had embedded YSOs, which would imply a timescale for their optically identified, starless cores 3 times longer than the duration of the protostellar stage. A comparison between the numbers from this study and those of Lee & Myers therefore suggests that the SCUBA maps only detect the denser stages in the evolution of prestellar cores, whereas the sample of optically identified cores by Lee & Myers also includes less evolved cores. In a study of more dense NH$_3$ cores, Jijina et al. (1999) found that the ratio of starless to stellar cores was close to unity or lower in a wide range of environments, likewise implying similar timescales for the evolution through the pre- and protostellar stages. Kirk et al. (2005) observed a large sample of 52 starless NH$_3$ cores with SCUBA and found that the cores that were bright at submillimeter wavelengths (i.e., having peak 850 μm flux densities larger than 170 mJy beam^{-1}) constituted approximately half of the cores detected by SCUBA and that the cores detected by SCUBA constituted approximately half of all the studied NH$_3$ cores. Comparison across such different samples should naturally be treated with care, dealing with systematic uncertainties, selection effects, etc. The big strength of the sample forming the basis of this paper is again that the sources are selected from one large-scale systematic and relatively unbiased set of observations with uniform sensitivity.

Assuming a typical lifetime of the deeply embedded stages studied here of 1×10^5 yr,[6] the total duration of the starless core stage would be 3×10^5 yr, with the SCUBA maps revealing the last 1×10^5 yr of this evolution, during which the central density increases above 5×10^4–1×10^5 cm^{-3} (J. Kirk 2005; H. Kirk 2006). As pointed out by Lee & Myers (1999), these timescales are significantly shorter than those for typical ambipolar diffusion models, unless the cores are marginally subcritical (Ciolek & Basu 2001). They are similar to the timescale for depletion in protostellar cores of $10^{5\pm0.5}$ yr derived by Jørgensen et al. (2005a) based on the measurements of chemical profiles of pre- and protostellar cores, again suggesting that the SCUBA dust condensations reflect the stage of prestellar cores where the density is high and significant depletion can start to occur.

We can naturally also compare these numbers to the timescales for the later stages of protostellar evolution. As pointed out above, the objects identified here represent YSOs in their first 10^5 yr of evolution and are an important addition to the sample of Jørgensen et al. (2006). That study was missing some

of these deeply embedded objects, but was more complete in terms of evolved Class I and Class II objects, which evolve over timescales of approximately 10^6 yr. The number of sources in this list compared to those of Jørgensen et al. (2006) appears to be consistent with the ratio between those timescales of about 10:1, or alternatively, if we accept those timescales as "known," we can say that star formation in Perseus has occurred at a fairly constant rate, continuing to current times.

4.3.3. Star Formation Efficiency

We can take the arguments a step further and estimate the star formation efficiency of the submillimeter cores and the entire cloud complex. Given the amount of mass in each core from the submillimeter observations, the star formation efficiency can be estimated as

$$\text{SFE} = \frac{M_{\text{YSO}}}{M_{\text{YSO}} + M_{\text{core}}}, \qquad (3)$$

where M_{YSO} is the mass of the newly formed stars and M_{core} is the mass of the cores. The total mass of the 72 SCUBA cores in the Perseus cloud was found to be $M_{\text{core}} = 37 \, M_\odot$ (Kirk et al. 2006), and, counting only those YSOs within 15″ of one of these submillimeter cores, we find 43 YSOs. Assuming that the masses of the newly formed stars are 0.3–0.5 $M_\odot$, the star formation efficiency for the entire Perseus cloud complex is estimated to be $\approx$10%–15%. This is comparable to the star formation efficiency of the nearby cluster-forming regions (Lada & Lada 2003). Approximately half of the total core mass in the cloud resides in the cores in NGC 1333, but by doing the same calculation as above, the star formation efficiency for just those cores is found to be similar to the value for the entire cloud. This again implies that significant star formation is currently occurring in the cores "outside" the main NGC 1333 and IC 348 clusters, in the dense regions associated with L1448, L1455, Barnard 1, and Barnard 5, among others, similar to the conclusion of Jørgensen et al. (2006). It should be noted that the mass estimates are sensitive to the assumptions about the dust temperature and the dust opacities and that the observational techniques are more or less sensitive to extended structure, for example.

The star formation efficiency quoted above is an estimate of the current core star formation efficiency and does not represent the actual efficiency of assembling the cores from the overall cloud environment. As pointed out by Kirk et al. (2006; see also Johnstone et al. [2004] for a similar result for the Ophiuchus molecular cloud complex), only a small fraction ($<$0.5%) of the total cloud mass resides in these dense cores, with the main fraction ($>$85%) of the cloud mass from the extinction maps ($\approx$18,500 $M_\odot$; Kirk et al. 2006) distributed at low $A_V < 5$. That number cannot be compared to the current mass of deeply embedded protostars from this analysis; a high number of YSOs have already formed in the Perseus molecular cloud with, for example, Jørgensen et al. (2006) identifying a "high quality" sample of 400 YSOs of Class II or earlier. These *Spitzer* observations are, furthermore, not picking out a significant number of more evolved, i.e., Class III, YSOs with a smaller amount of infrared excesses. With these higher numbers of YSOs distributed over all evolutionary stages and the total cloud mass, the time-averaged star formation efficiency over the entire evolution of the cloud until the present time is probably closer to a few percent, which includes the efficiency of assembling cores from the overall cloud dust mass in the first place and, subsequently, the efficiency of these cores actually forming stars. In this context, it should also be emphasized that the observed mass distribution of SCUBA core masses is a current snapshot

---

[6] Ward-Thompson et al. (2007) quote a best estimate of the timescale of the evolution of YSOs through the embedded phases of $(2 \pm 1) \times 10^5$ yr from previous studies, which includes parts of the "less embedded" Class I stages for which the cores associated with the YSOs are not picked up by the SCUBA surveys.

of potentially star-forming cores. With their lifetimes of about 10^5 yr (§ 4.3.2), it is not unreasonable to expect that at least 10 times as many cores have previously existed in the cloud and formed what are currently observed as Class II and III YSOs.

5. CONCLUSIONS

This paper has presented a comparison between the dust condensations from SCUBA maps and mid-infrared sources from *Spitzer* observations. This study represents a large systematic census of the embedded YSO population and thereby allows statements from a large sample of sources. The main conclusions of this paper are:

1. The mid-infrared sources with 24 μm detections and red colors are found to be located close to the center of the SCUBA cores mapped by Kirk et al. (2006), typically within 15″ (less than half a core radius) of their peaks. The sources are found to have characteristic red colors, with $[3.6] - [4.5] > 1.0$ and $[8.0] - [24] > 4.5$, but do not show similarly red $[5.8] - [8.0]$ colors. The most deeply embedded objects are found in regions with high extinction, $A_V \geq 5$ (90% of the objects with $[3.6] - [4.5] > 2$), similar to the extinction threshold for the SCUBA cores. Still, the red colors are not purely an effect of cloud extinction.

2. All the SCUBA cores with high "concentrations" have embedded YSOs, but also a nonnegligible number of cores with low concentrations have embedded YSOs, making this distinction ambiguous. A few of the strongest sources in NGC 1333 are not picked up by the above criteria described under point 1 due to saturation and confusion. The cores associated with those sources can be picked out by their high concentrations and submillimeter fluxes.

3. From the above considerations, a relatively unbiased sample of deeply embedded YSOs can be constructed. In this fashion, we identify 49 embedded YSOs associated with SCUBA cores from the list of Kirk et al. (2006). Out of 72 SCUBA cores, 40 are found to have associated MIPS sources (including four cores, which are associated with saturated MIPS sources not included in the c2d catalog). Only three SCUBA cores are found to have more than one MIPS sources within 15″.

4. The narrowness of the spatial distribution of red sources within the SCUBA cores suggests that the velocities of the newly formed protostars relative to the cores are low, close to the isothermal sound speed. This argues against the suggestion that the motions of protostars relative to the ambient cloud regulate the timescale over which significant accretion can occur.

5. From the number of SCUBA cores with and without embedded YSOs (40 and 32, respectively), the timescale of the evolution through the dense prestellar stages, where the cores are recognized in the submillimeter maps and their central densities are larger than 5×10^4–1×10^5 cm^{-3}, is similar to the timescale for evolution through the embedded protostellar stages. This result further implies that the observable SCUBA core stage constitutes one-third of the lifetime of less dense prestellar cores, e.g., those picked up in optical or NH_3 surveys.

6. The current star formation efficiency estimated from the mass of the embedded protostars and the SCUBA cores is found to be $\approx$10%–15%, similar to the star formation efficiency of the nearby star-forming clusters. If we also take into account the efficiency of assembling the cores in the first place, the total star formation efficiency is a few percent.

The survey presented in this paper places important constraints on the formation mechanisms, which should be taken into account in theoretical studies of low-mass star formation. Naturally, many interesting problems remain, which can be pursued using the results of this paper as a starting point, for example, a more detailed characterization of the individual star-forming cores (e.g., studying variations in dynamics from molecular line widths and/or chemical signatures) and of the embedded YSOs (e.g., their physical properties/evolutionary stage by completing their SEDs from near-infrared through [sub]millimeter wavelengths). It will also be interesting to test whether the criteria from this paper can be used to build comparable samples of starless and star-forming cores in other nearby clouds. This will test whether the differing physical conditions, such as the external pressure, in different star-forming regions affects whether a given core forms stars or not. This might, for example, reflect a different value for the concentration above which all submillimeter cores in a given region are found to have embedded protostars. In that sense, this paper will serve as a starting point for such studies and for similar censuses of other clouds surveyed at mid-infrared and (sub)millimeter wavelengths.

REFERENCES

Allen, L. E., et al. 2004, ApJS, 154, 363
André, P., Ward-Thompson, D., & Barsony, M. 1993, ApJ, 406, 122
———. 2000, in Protostars and Planets IV, ed. V. Mannings, A. P. Boss, & S. S. Russell (Tucson: Univ. Arizona Press), 59
Ayliffe, B. A., Langdon, J. C., Cohl, H. S., & Bate, M. R. 2007, MNRAS, in press (astro-ph/0611421)
Ballesteros-Paredes, J., Klessen, R., Mac Low, M.-M., & Vázquez-Semadeni, E. 2007, in Protostars and Planets V, ed. B. Reipurth, D. Jewitt, & K. Keil (Tucson: Univ. Arizona Press), 63
Bate, M. R., Bonnell, I. A., & Bromm, V. 2003, MNRAS, 339, 577
Bondi, H., & Hoyle, F. 1944, MNRAS, 104, 273
Bonnell, I. A., Bate, M. R., Clarke, C. J., & Pringle, J. E. 1997, MNRAS, 285, 201
Bonnell, I. A., Clarke, C. J., Bate, M. R., & Pringle, J. E. 2001, MNRAS, 324, 573
Ciolek, G. E., & Basu, S. 2001, ApJ, 547, 272
Crapsi, A., Caselli, P., Walmsley, C. M., Myers, P. C., Tafalla, M., Lee, C. W., & Bourke, T. L. 2005, ApJ, 619, 379

Di Francesco, J., Evans, N. J. I., Caselli, P., Myers, P. C., Shirley, Y., Aikawa, Y., & Tafalla, M. 2007, in Protostars and Planets V, ed. B. Reipurth, D. Jewitt, & K. Keil (Tucson: Univ. Arizona Press), 17
Enoch, M. L., et al. 2006, ApJ, 638, 293
Evans, N. J., Rawlings, J. M. C., Shirley, Y. L., & Mundy, L. G. 2001, ApJ, 557, 193
Evans, N. J., et al. 2003, PASP, 115, 965
———. 2005, in Delivery of Data from the c2d Legacy Project: IRAC and MIPS (Pasadena: SSC)
Goodman, A. A., et al. 2004, in ASP Conf. Proc. 323, Star Formation in the Interstellar Medium, ed. D. Johnstone et al. (San Francisco: ASP), 171
Greene, T. P., Wilking, B. A., Andre, P., Young, E. T., & Lada, C. J. 1994, ApJ, 434, 614
Hartmann, L. 2002, ApJ, 578, 914
Hatchell, J., Richer, J. S., Fuller, G. A., Qualtrough, C. J., Ladd, E. F., & Chandler, C. J. 2005, A&A, 440, 151

Hogerheijde, M. R., & Sandell, G. 2000, ApJ, 534, 880
Jijina, J., Myers, P. C., & Adams, F. C. 1999, ApJS, 125, 161
Johnstone, D., & Bally, J. 2006, ApJ, 653, 383
Johnstone, D., Di Francesco, J., & Kirk, H. 2004, ApJ, 611, L45
Johnstone, D., Wilson, C. D., Moriarty-Schieven, G., Joncas, G., Smith, G.,
    Gregersen, E., & Fich, M. 2000, ApJ, 545, 327
Jørgensen, J. K., Schöier, F. L., & van Dishoeck, E. F. 2002, A&A, 389, 908
———. 2005a, A&A, 435, 177
Jørgensen, J. K., et al. 2005b, ApJ, 631, L77
———. 2006, ApJ, 645, 1246
Kirk, H., Johnstone, D., & Di Francesco, J. 2006, ApJ, 646, 1009
Kirk, J. M., Ward-Thompson, D., & André, P. 2005, MNRAS, 360, 1506
Lada, C. J. 1987, in IAU Symp. 115, Star Forming Regions, ed. M. Peimbert &
    J. Jugaku (Dordrecht: Reidel), 1
Lada, C. J., & Lada, E. A. 2003, ARA&A, 41, 57
Ladd, E. F., Myers, P. C., & Goodman, A. A. 1994, ApJ, 433, 117
Lee, C. W., & Myers, P. C. 1999, ApJS, 123, 233

Motte, F., André, P., & Neri, R. 1998, A&A, 336, 150
Muzerolle, J., et al. 2004, ApJS, 154, 379
Ossenkopf, V., & Henning, T. 1994, A&A, 291, 943
Rebull, L., et al. 2006, ApJ, submitted
Ridge, N. A., et al. 2006, AJ, 131, 2921
Shirley, Y. L., Evans, N. J., & Rawlings, J. M. C. 2002, ApJ, 575, 337
Tapia, M., Persi, P., Bohigas, J., & Ferrari-Toniolo, M. 1997, AJ, 113, 1769
Walawender, J., Bally, J., Kirk, H., & Johnstone, D. 2005, AJ, 130, 1795
Walawender, J., Bally, J., Kirk, H., Johnstone, D., Reipurth, B., & Aspin, C.
    2006, AJ, 132, 467
Walsh, A. J., Myers, P. C., & Burton, M. G. 2004, ApJ, 614, 194
Ward-Thompson, D., André, P., Crutcher, R., Johnstone, D., Onishi, T., &
    Wilson, C. 2007, in Protostars and Planets V, ed. B. Reipurth, D. Jewitt, &
    K. Keil (Tucson: Univ. Arizona Press), 33
Whitney, B. A., Wood, K., Bjorkman, J. E., & Cohen, M. 2003, ApJ, 598, 1079
Williams, J. P., de Geus, E. J., & Blitz, L. 1994, ApJ, 428, 693
Young, K. E., et al. 2006, ApJ, 644, 326